

An Efficient Meshless Approach to Multi-scale Modeling in the Time-domain

Yiqiang Yu^{1,2}, Farid Jolani², and Zhizhang (David) Chen²

¹School of Information Engineering
East China Jiaotong University, Nanchang, China
yiqiang.yu@dal.ca

²Department of Electrical and Computer Engineering
Dalhousie University, Halifax, Canada
farid.jolani@dal.ca; z.chen@dal.ca

Abstract — An efficient multi-scale approach to meshless modeling of three-dimensional guided wave problems is realized by hybridization of the radial point interpolation method (RPIM) and the unconditionally stable leapfrog alternating-direction implicit (ADI-) RPIM scheme. In it, the solution domain is regionalized; the leapfrog ADI-RPIM is applied to regions with coarse nodal distributions while the original RPIM is applied to the rest of the dense nodal solution domain. With application of the leapfrog ADI scheme, a uniform time-step can now be applied to the entire solution domain without temporal and spatial interpolation between different computational regions. Furthermore, in the proposed scheme, implicit updating of field variables is confined only within the regions of densely-distributed nodes, yielding a significant saving in memory overhead and a further reduction in CPU time in comparison with leapfrog ADI-RPIM and original RPIM, respectively.

Index Terms — Alternating-direction implicit scheme, finite-difference time-domain, hybrid methods, meshless methods, radial point interpolation method.

I. INTRODUCTION

With recent advances in modern electronic and electrical technologies, electromagnetic problems are becoming exceedingly complex; as a result, modern computer-aided tools based on

conventional computational electromagnetic methods often experience difficulties in providing accurate modeling solutions within a reasonable time. To tackle the problem, higher-order basis functions along with mesh reduction techniques have been applied to the conventional methods to reduce memory and time consumption while maintaining the same level of modeling accuracy [1, 2]; or alternatively, novel numerical methods have been sought that can free constraints on numerical accuracy from the connectivity laws of grid nodes and shape and dimension of elementary cells that long exist in the conventional methods. One of the promising new numerical techniques is the meshless method. It utilizes a set of scattered nodes to represent a problem domain and associated boundaries, rather than a predefined mesh/grid as used in the conventional numerical methods.

Among the meshless techniques that have been adapted for use in computational electromagnetics, the radial point interpolation method (RPIM) [3] gains significant attention due to its simplicity, accuracy, and consistency. Its applications have been seen in one dimensional wave propagation problems [4], two-dimensional H-plane bent waveguides [5, 6], and three-dimensional cavity problems [7]. Recently, the method has been extended to electromagnetic radiation and scattering problems in open-region [8] and with material interfaces [9]. Although the method has been repeatedly reported to be much more robust than the conventional finite-difference

time-domain (FDTD) method, computational performance of the method is somehow limited by its stability constraint on time step; this is a drawback from the employment of explicit finite-difference scheme to approximate the time derivatives in Maxwell's equations. Efforts were thus made in our previous work [10, 11] to further improve the computational efficiency of the method, with the implementation of leapfrog alternating-direction-implicit (ADI) scheme [12-15] to remove the stability constraint; it leads to an unconditionally stable meshless ADI-RPIM method.

Computational efficiency of the unconditionally stable meshless ADI-RPIM method has then been assessed with a large number of numerical experiments. It is observed that the used implicit meshless scheme is very attractive for the problems where nodes are highly irregularly distributed over an entire solution domain.

However, when irregular nodal distributions are applied only in a small portion of the problem domain, the method appears to be less efficient. Further analysis of the computational expenditures leads to the explanation: since the method is based on the implicit updates of field variables, extra computational cost is required for matrix assembly of extra off-diagonal terms in coefficient matrix and the associated matrix computation during the time-marching; depending on the average number of nodes that are enclosed in the support domain for interpolation, this process can sometimes become time-consuming and compromise the overall computational efficiency of the unconditional meshless scheme.

Therefore, it is desirable to develop a smart hybrid approach that applies the unconditionally stable meshless method intelligently. To this end, in this paper, we propose the approach that applies the efficient leapfrog ADI-RPIM only to computational sub-regions with dense nodal distributions and the original RPIM to the rest of the problem domain. In such a way, the extra memory required to store the off-diagonal terms of the matrix equations and the additional CPU time for matrix computations can be minimized. Thanks to the multi-scale modeling capability of the meshless RPIM, such a hybridization can be realized easily without need of sub-gridding and additional spatial interpolation. Moreover, due to

the alternating nature of the field variables in leapfrog ADI-RPIM, temporal interpolation is not needed either.

In the next section, we will first briefly describe the RPIM method in three dimensions and then present a set of RPIM equations with the convolutional perfectly matched layer (CPML) absorbing boundary conditions. In Section 3, we will present the unconditional stable RPIM method with the corresponding leap-frog ADI-RPIM equations and then combine it with the original explicit RPIM to formulate the hybrid approach; In Section 4, we will numerically validate the effectiveness of the proposed approach; the comparison between the proposed hybrid approach, the original RPIM method, the leapfrog ADI-RPIM, and the conventional FDTD in terms of computational cost is shown.

II. THE MESHLESS RPIM METHOD

The formulation of the meshless RPIM in computing electromagnetic fields comprises three key steps: representation of field variables with the point interpolation scheme, construction of shape functions, and discretization of Maxwell's time-dependent equations.

A. The Local Point Interpolation Scheme and Shape Function

The node-based RPIM method discretizes a solution domain using a set of spatial nodes. As seen in Fig. 1, an arbitrary solution domain is filled with scattered nodes; whereas, the boundary of the domain is precisely represented with lying-on nodes. The underlying point interpolation scheme interpolates the field variable u at point q locally with and only with its values at surrounding nodes. A support domain S is defined for each q to enclose N points that are used for interpolation. The values of parameter N in the range of 4-12 are used throughout this work. Mathematically, such interpolation can be expressed as:

$$u(X) = \sum_{n=1}^N r_n(X) a_n + \sum_{m=1}^M p_m(X) b_m, \quad (1)$$

where $X=(x_q, y_q, z_q)$ is the coordinate of point q , $r_n(X)$ is the radial basis function, $p_m(X)$ is the monomial basis function, and a_n and b_m are the associated interpolation coefficients.

The radial basis function in a Gaussian form is deployed in our work to weight the contributions

will become unstable and give rise to divergent numerical results. The stability limit on the time-steps used in the original meshless RPIM method is extracted from [7] and listed here for completeness.

$$\Delta t \leq \frac{2}{\text{sqrt}(|\lambda_{\max}(\mathbf{Q})|)}, \quad (13)$$

where $\lambda_{\max}(\mathbf{Q})$ is the largest eigenvalue of matrix \mathbf{Q} in terms of magnitude; and $\mathbf{Q}=\mathbf{CB}+\mathbf{DA}$, where \mathbf{A} , \mathbf{B} , \mathbf{C} , and \mathbf{D} are the coefficient matrices associated with the right-hand-side of the meshless RPIM formulation.

The conditional stability expressed by (16) is due to employment of the explicit finite-difference approximation to the time derivatives in Maxwell's equations. In order to eliminate the stability constraint and consequently improve the computational efficiency with a larger step, a leapfrog version of the ADI scheme is incorporated into the RPIM method in [10], leading to an unconditionally stable *leapfrog* ADI-RPIM meshless method. The resultant scheme is implicit that requires solving a band matrix at each time iteration. The formulations for the implicit update of field components E_x and H_z are extracted from [10] and are listed below for simplicity and completeness.

$$E_{x,i}^{n+\frac{1}{2}} - \frac{\Delta t^2}{4\mu\epsilon} \sum_j \sum_k E_{x,k}^{n+\frac{1}{2}} \partial_y \Phi_k \partial_y \Phi_j = E_{x,i}^{n-\frac{1}{2}} - \frac{\Delta t^2}{4\mu\epsilon} \sum_j \sum_k E_{x,k}^{n-\frac{1}{2}} \partial_y \Phi_k \partial_y \Phi_j + \frac{\Delta t}{\epsilon} \left(\sum_j H_{z,j}^n \partial_y \Phi_j - \sum_j H_{y,j}^{n+1} \partial_z \Phi_j \right). \quad (14)$$

$$H_{z,i}^{n+1} - \frac{\Delta t^2}{4\mu\epsilon} \sum_j \sum_k H_{z,k}^{n+1} \partial_x \Phi_k \partial_x \Phi_j = H_{z,i}^n - \frac{\Delta t^2}{4\mu\epsilon} \sum_j \sum_k H_{z,k}^n \partial_x \Phi_k \partial_x \Phi_j + \frac{\Delta t}{\mu} \left(\sum_j E_{x,j}^{n+\frac{1}{2}} \partial_y \Phi_j - \sum_j E_{y,j}^{n+\frac{1}{2}} \partial_x \Phi_j \right). \quad (15)$$

Here the range of values that correspond to indices k and j depends on the number of neighboring nodes enclosed in the local support domain of the node i . For instance, when $N=4$, the values of k and j are in the range of 1- 4, and the i th row of resultant band coefficient matrix will have 9 nonzero elements.

IV. THE PROPOSED HYBRID MESHLESS ADI-RPIM SCHEME

In the proposed hybrid scheme, a solution domain is divided into a number of sub-domains that are categorized into dense node regions and coarse node regions. A node i is considered to be in a dense node region when ratio of the average nodal spacing 'AD' in the local support domain of node i to the average distance between two adjacent nodes over the entire solution domain falls below a pre-determined threshold; an optimized search routine is developed and applied to decide appropriate boundaries of those sub-regions.

The leapfrog ADI-RPIM is then applied to the dense node sub-regions; whereas, the original RPIM is applied to the remaining coarse node regions. For nodes lying at a region interface, field values are computed with the ADI-RPIM scheme. As can be seen from (15)-(16), E-field, and H-field in the leapfrog ADI-RPIM are staggered in time in the same manner as RPIM; synchronization of the time steps of dense regions and outer coarse regions can thus be realized without temporal interpolation. As for any node with a support domain intercepting with a region interface, update of field values needs to access the current field values at some of the nodes that fall into the another region; in this case, it is more convenient to recast the explicit RPIM update equations into a format of matrix equation and combine it with the matrix equation derived from the implicit leapfrog ADI-RPIM scheme. More specifically, combination of (4) with (15), and (5) with (16) yields two new matrix equations expressed as

$$\mathbf{A}\mathbf{E}_x^{n+\frac{1}{2}} = \mathbf{A}\mathbf{E}_x^{n-\frac{1}{2}} + \mathbf{B}\mathbf{H}_z^n - \mathbf{C}\mathbf{H}_y^n + \boldsymbol{\Psi}_E, \quad (16)$$

$$\text{and } \mathbf{M}\mathbf{H}_z^{n+1} = \mathbf{M}\mathbf{H}_z^n + \mathbf{D}\mathbf{E}_x^{n+\frac{1}{2}} - \mathbf{G}\mathbf{E}_y^{n+\frac{1}{2}} + \boldsymbol{\Psi}_H, \quad (17)$$

where entries of coefficient matrices \mathbf{A} , \mathbf{B} , \mathbf{C} , \mathbf{M} , \mathbf{D} and \mathbf{G} , and auxiliary vector $\boldsymbol{\Psi}$ due to the CPML can be found from (4) to (16).

V. NUMERICAL EXPERIMENTS

A. 5-Pole H-Plane Iris Filter

The return loss of a bandpass waveguide iris filter was computed to illustrate the numerical efficiency of the hybrid meshless method presented here. The filter was based on a WR-28

rectangular waveguide for millimeter-wave applications. It consists of 5 cavities formed with 6 sets of thin perpendicular conductive walls. To evaluate performance of the filter under single-mode propagation, a plane source with TE_{10} field distribution was used to excite TE_{10} mode. The sensor nodes were placed at a short distance from the sources to record electric field component E_z . The geometry and solution domain setup of the problem are shown in Fig. 2, whereas the dimension of the filter is given in Table 1.

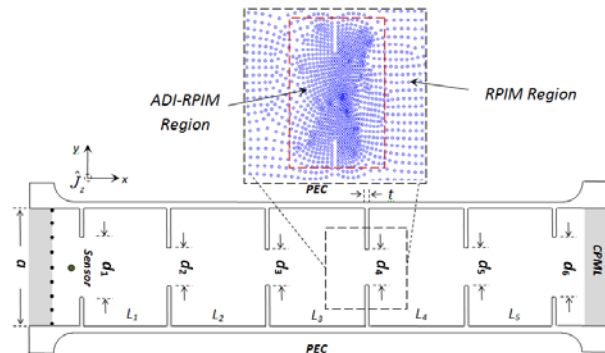


Fig. 2. A 5-pole H-plane iris filter (WR-28 waveguide).

Table 1: Dimension of the iris filter (inches)

a	t	L_1	L_2	L_3	L_4	L_5
0.28	0.008	0.169	0.187	0.192	0.187	0.169
d_1	d_2	d_3	d_4	d_5	d_6	
0.127	0.082	0.077	0.077	0.082	0.127	

Here a is the width of the WR-28 rectangular waveguide, t is the thickness of the irises, L_i specifies the space between two adjacent irises, and d_i defines the gap between a set of irises.

Due to the small dimension of the thin iris, a very fine uniform grid will be needed to discretize the entire problem when the conventional FDTD is used; this yields a significant number of unknowns to be solved with large computational effort. However, with the multi-scale modeling capability of the meshless RPIM, a set of densely distributed nodes can now be placed in the regions around thin walls for refined solutions; the rest of the problem domain remains represented with uniformly distributed coarse nodes, as shown in Fig. 2.

Then, a computational sub-domain is defined to enclose those densely distributed nodes where the field values are updated with unconditionally

stable ADI-RPIM scheme. The rest of the domain is still solved with the original RPIM method.

To accurately assess the S11 values of the iris filter shown in Fig. 2, a reference problem with the same nodal discretization but with the irises removed and top/bottom PECs replaced by CPML layers is also simulated. The total electric field recorded at the sensor point due to the iris walls is Fourier transformed to the frequency domain and compared with the incident field computed from the reference problem to determine the reflected field and thus the numerical reflection at *port1*.

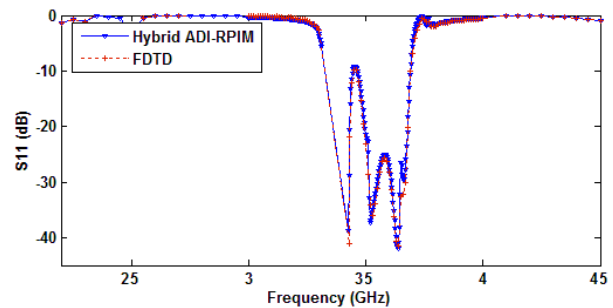


Fig. 3. Computed S11 parameters of 5-pole H-plane iris filter.

Figure 3 shows the computed S11 values for the frequency sweep from 22 GHz to 45 GHz. As can be seen, the results solved with the proposed hybrid meshless scheme agree well with the reference solution from the conventional FDTD with a fine grid; both indicate a good performance of the filter design with the center frequency of 35.2GHz and the bandwidth of 3.2GHz; the reflection in the pass band is lower than -10dB.

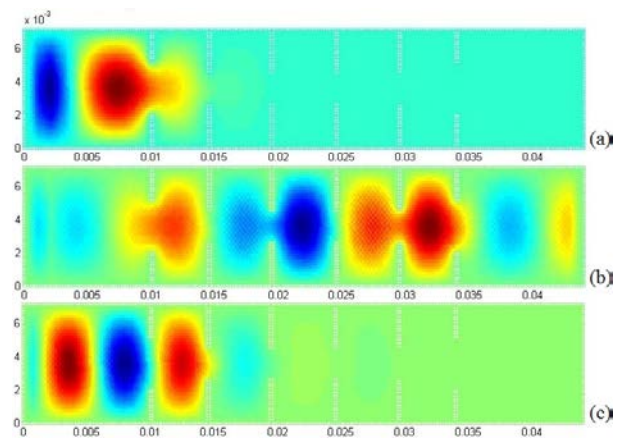


Fig. 4. E-field distributions at different frequencies (after 20000 time-steps), (a) at 30 GHz (below the low end of the pass band); (b) 35.5 GHz (inside the pass band); (c) 40 GHz (beyond the pass band).

Figure 4 presents the graphical displays of E-field distribution along the waveguide filter after 20000 time iterations at different frequencies. As clearly seen, within the pass-band, the steady-state TE₁₀ mode propagation is established with little reflection, whereas outside the pass-band, the E-field attenuates and eventually vanishes as it propagates away from the sources.

B. Substrate Integrated Waveguide (SIW)

The second example was the simulation of the steady-state transmission mode of a single-layer substrate integrated waveguide (SIW). Figure 5 shows the geometrical design and fundamental parameters of the SIW under study. For illustration purposes, a standard substrate for high speed digital applications, N-4000-13, with $\epsilon_r = 3.6$ and height $h = 16$ mil, was used.

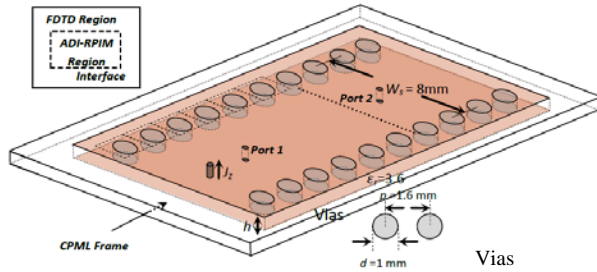


Fig. 5. A 2D substrate integrated waveguide.

In principle, the substrate integrated waveguide emulates a dielectric-filled waveguide with lateral walls formed by rows of vias that are sufficiently close to each other. If properly designed, the behavior of a SIW is similar to that of a conventional rectangular waveguide. The theoretical cutoff frequency of the SIW shown in Fig. 5 was found to be around 10GHz with the following formulae from [18]:

$$f_c = \frac{c}{2W_d\sqrt{\epsilon_r}}, \text{ and } W_d = W_s - \frac{d^2}{0.95p} + 0.1\frac{d^2}{W_s} \quad (18)$$

where c is the speed of light, ϵ_r is the dielectric constant, W_s is the width of the waveguide, W_d is the effective width of the guide, d the diameter of the via, and p is distance between the vias.

Since the SIW can only support TE_{m0} modes due to dielectric gaps created by the via separations, a vertically oriented probe was used to excite the waveguide. The uniform current density along the probe was expressed with a ramped sinusoidal function (20). The duration of the ramp

function was set to be six cycles of the sinusoidal pulse to eliminate the switch-on noise. The long-time response of the waveguide to such an excitation was approximately monochromatic.

$$J_z(t) = R(t - 2T_0) \cdot \sin(2\pi f_0(t - 2T_0))\hat{z}. \quad (19)$$

The ratio of voltages at port 1 and port 2 indicates the transmission behavior of the SIW under study and it was firstly examined. The time-domain profiles of electric field along the two ports were recorded up to 30000 time iterations and Fourier-transformed to obtain the corresponding frequency responses; and then line-integrations were performed along the ports to obtain the voltage values at the two ports. As can be seen from Fig. 6, the results computed with the hybrid approach are in good agreement with the reference solution from the FDTD, both indicating a cut-off frequency of 10GHz for the dominant mode (TE₁₀) of the SIW.

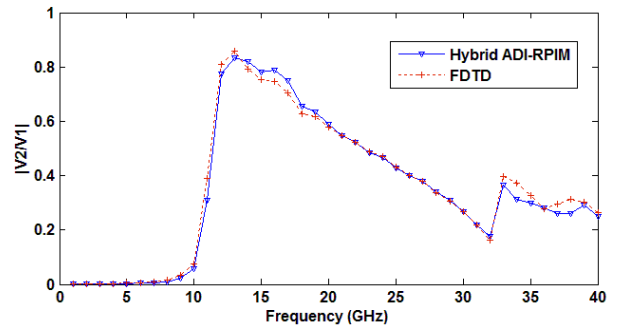


Fig. 6. Ratio of voltages across two ports (1-40 GHz).

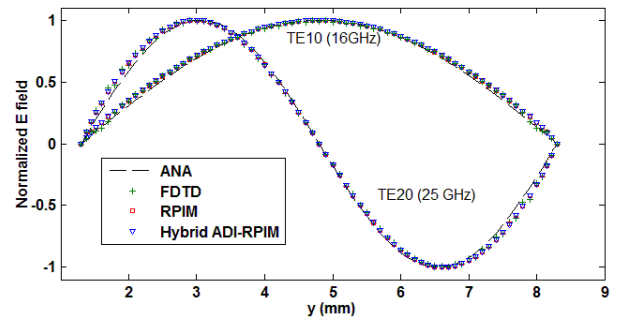


Fig. 7. Normalized electric field along the line of observation points.

The steady-state field distribution over the SIW for higher TE modes was also examined. To launch a TE₂₀ propagating mode along the SIW, the waveguide was excited with two probes, which were positioned at 1/4 and 3/4 of the width of the waveguide, in an anti-phase manner. Figure 7

shows the normalized electric field along the line of observation points depicted in Fig. 6 for different TE modes. The computed results are compared with the ones from the FDTD of a fine uniform grid, the original RPIM and the analytical values from an equivalent dielectric filled rectangular waveguide. Good agreements are observed.

Figure 8 presents snapshots of steady-state E field distribution over the SIW for other TE modes, computed with proposed hybrid ADI-RPIM approach after 500,000 time steps. As can be seen, the results do not suffer from late-time instability and there are no noticeable reflections from the dense/coarse region interface that often exist in a conventional sub-gridding scheme with additional interpolation at the region interface.

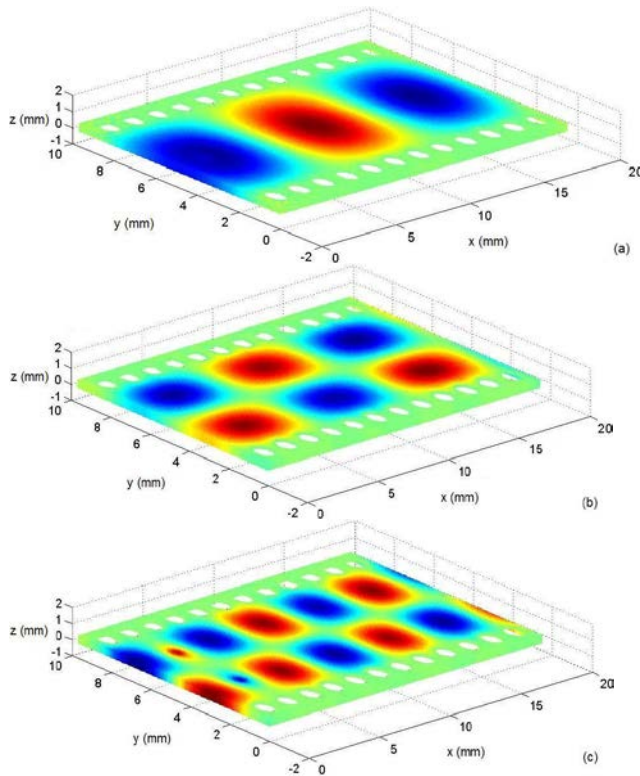


Fig. 8. Steady-state TE mode propagation over the substrate integrated waveguide, (a) TE_{10} mode at 16 GHz; (b) TE_{20} mode at 25 GHz; (c) TE_{20} mode at 30 GHz.

VI. COMPUTATIONAL EXPENDITURE

To quantify the numerical performance of the proposed hybrid ADI-RPIM meshless approach, computational expenditure of the first numerical example is monitored and tabulated in Table 2.

The original RPIM, the ADI-RPIM, along with the orthogonal FDTD are included for comparison. As clearly seen, all three meshless methods outperform the conventional FDTD in CPU time as expected; with the FDTD method, a very fine uniform grid is needed to discretize the entire solution domain due to the small dimension of the thin iris; this yields a very large number of total number of unknowns to be solved.

Among the three meshless methods, it is interesting to observe that the pure non-hybrid leapfrog ADI-RPIM does not significantly reduce the CPU run-time and the efficiency gained from its unconditionally stability is compromised by the additional computational cost required for matrix assembly of extra off-diagonal terms and matrix computation during the time-marching. However, the proposed hybrid approach not only saves more than 50% of the memory required by a pure non-hybrid unconditionally stable ADI-RPIM but also runs 100% faster.

Table 2: Computational expenditure of example A

	FDTD	RPIM	ADI-	Hybrid
Unknowns	176562	34581	34581	34581
CPU time (sec.)	512	125	121	56
Memory (Mbs)	364	111	319	152
CPU gain	1	3.0	3.2	8.1

VII. CONCLUSION

The presented hybrid ADI-RPIM approach further improves the computational efficiency of the meshless RPIM technique for solving problems with fine geometric features. With the unconditionally stable ADI-RPIM method only applied to the computational regions that require fine discretization (to describe abrupt changes in field values or geometrical details), CPU, and memory overhead due to implicit updates of field variables are minimized, which in turn renders a CPU gain over the original RPIM meshless method. In addition, time-steps at different computational regions can be synchronized without temporal interpolation; as well, the underlying point interpolating nature of the RPIM method obviates the need of additional spatial interpolation at region interfaces. The numerical experiments show the proposed hybrid meshless approach remains numerically stable after half a million time iterations.

ACKNOWLEDGMENT

The work was supported in part by the National Natural Science Foundation of China (NSFC) fund under contract 61061003 and Natural Science and Engineering Research Council of Canada under contract 155230-07.

REFERENCES

- [1] R. K. Gordon and W. E. Hutchcraft, "The Use of Multiquadric Radial Basis Functions in Open Region Problems," *Applied Computational Electromagnetics Society (ACES) Journal*, vol. 21, no. 2, pp. 127 – 134, July 2006.
- [2] A. B. Ali, E. A. Hajlaoui, and A. Gharsallah, "Efficient Analysis Technique for Modeling Periodic Structures Based on Finite Element Method using High-Order Multiscale Functions," *Applied Computational Electromagnetics Society (ACES) Journal*, vol. 25, no. 9, pp. 755 - 763, September 2010.
- [3] J. G. Wang and G. R. Liu, "A Point Interpolation Meshless Method Based on Radial Basis Functions," *Int. J. Numer. Methods Eng.*, 2001.
- [4] S. J. Lai, B. Z. Wang, and Y. Duan, "Meshless Radial Basis Function Method for Transient Electromagnetic Computations," *IEEE Trans. Magnetics*, vol. 44, no. 10, pp. 2288-2295, 2008.
- [5] T. Kaufmann, C. Fumeaux, and R. Vahldieck, "The Meshless Radial Point Interpolation Method for Time-Domain Electromagnetic," *IEEE MTT-S Int. Microwave Symp. Dig.*, Atlanta GA, pp. 61-64, June 15-20, 2008.
- [6] S. J. Lai, B. Z. Wang, and Y. Duan, "Solving Helmholtz Equation by Meshless Radial Basis Functions Method," *Progress In Electromagnetics Research B*, vol. 24, pp. 351-367, 2010.
- [7] Y. Yu and Z. Chen, "A Three-Dimensional Radial Point Interpolation Method for Meshless Time-Domain Modeling," *IEEE Trans. Microwave Theory & Techniques*, vol. 57, no. 8, pp. 2015-2020, 2009.
- [8] Y. Yu and Z. Chen, "Meshless RPIM Modeling of Open-Structures using PMLs," *IEEE MTT-S Int. Microwave Symp. Dig.*, Anaheim, May 23-28, 2010.
- [9] Y. Yu and Z. Chen, "Implementation of Material Interface Conditions in the Radial Point Interpolation Meshless Method," *IEEE Trans. Antennas and Propagation*, vol. 59, no. 8, pp. 2916-2923, 2011.
- [10] Y. Yu and Z. Chen, "Towards the Development of Unconditionally Stable Time-Domain Meshless Numerical Methods," *IEEE Trans. Microwave Theory and Techniques*, vol. 58, no. 3, pp. 578-586, 2010.
- [11] T. Kaufmann, Y. Yu, C. Engström, Z. Chen, and C. Fumeaux "Recent Developments of the Meshless Radial Point Interpolation Method for Time-Domain Electromagnetics," *International Journal of Numerical Modelling: Electronic Networks, Devices and Fields*, Article first published online :, DOI: 10.1002/jnm.1830, Feb. 15, 2012.
- [12] S. J. Cooke, M. Botton, T. M. Antonsen, and B. Levush, "A Leapfrog Formulation of the 3D ADI-FDTD Algorithm," *Intl. Workshop on Computational Electromagnetics in Time-Domain*, , pp. 1-4, Oct. 15-17, 2007
- [13] F. Zhen, Z. Chen, and J. Zhang, "Toward the Development of a Three-Dimensional Unconditionally Stable Finite Difference Time-Domain Method," *IEEE Trans. Microwave Theory & Techniques*, vol. 48, no. 9, pp. 1550-1558, Sept. 2000.
- [14] T. Namiki, "3-D ADI-FDTD Method--Unconditionally Stable Time-Domain Algorithm for Solving Full Vector Maxwell's Equations," *IEEE Trans. Microwave Theory & Techniques*, vol. 48, no. 10, pp. 1743-1748, Oct. 2000.
- [15] J. Chen and J. Wang, "An Unconditionally Stable Subcell Model for Thin Wires in the ADI-FDTD Method," *Applied Computational Electromagnetics Society (ACES) Journal*, vol. 25, no. 8, pp. 659 - 664, August 2010.
- [16] J. A. Roden and S. D. Gedney, "Convolutional PML (CPML): An Efficient FDTD Implementation of the CFS-PML for Arbitrary Media," *Microwave Opt. Technol. Lett.*, vol. 27, pp. 334-339, Dec. 5, 2000.
- [17] S. D. Gedney, G. Liu, J. Alan Rodden, and A. Zhu, "Perfectly Matched Layer Media with CFS for an Unconditionally Stable ADI-FDTD Method," *IEEE Trans. Antennas & Propagation*, vol. 49, no. 11, pp. 1554-1559, 2001.
- [18] F. Xu and K. Wu, "Guided-Wave and Leakage Characteristics of Substrate Integrated Waveguide," *IEEE Trans. Microwave theory & techniques*, vol. 53, no. 3, pp. 66-73, 2005.



Yiqiang Yu (M'09) received the M.Sc. degree (with distinction) in communication systems in 2003 and Ph.D. in microwave engineering in 2007 from Swansea University, U.K.

He is presently a full Professor with East China Jiaotong University. He is also a Research Fellow with the Department of Electrical and Computer Engineering, Dalhousie University, Halifax, Canada.

His primary interest is in applications of computational electromagnetics, in particular use of finite-difference methods, method of moments, and fast multipole methods in both the time and frequency domains. His interests also include RF/microwave components design, antennas design and measurement, EMI/EMC analysis and testing, and iterative solvers and preconditioning techniques for large-scale matrix computation.

Dr. Yu was a recipient of the Overseas Research Scholarship from the United Kingdom Overseas Research Award Program during 2004–2007.



Zhizhang (David) Chen (S'92-M'92-SM'96-F'10) received the Ph.D. degree from the University of Ottawa, ON, Canada.

He was a NSERC Postdoctoral Fellow with the ECE Department of McGill University, Montreal, Canada. He joined Dalhousie University, Halifax, Canada, in 1993, where he is presently a Professor. He has authored and coauthored over 200 journal and conference papers in computational electromagnetics and RF/microwave electronics. He was one of the originators in developing new numerical algorithms (including ADI-FDTD method) and in designing new classes of compact RF front-end circuits for wireless communications. His current research interests include numerical modeling and simulation, RF/microwave electronics, smart antennas, and wireless transceiving technology and applications.

Dr. Chen received the 2005 Nova Scotia Engineering Award, a 2006 Dalhousie graduate teaching award, 2006 ECE Professor of the Year award and the 2007 Faculty of Engineering Research Award from Dalhousie University.